Journal of Applied Biology & Biotechnology Vol. 14(6), pp. 49-64, November-December, 2026
Available online at http://www.jabonline.in
DOI: 10.7324/jabb.2026.310917

Visible-light-activated chlorophyllin–calcium phosphate nanohybrid for reusable photodynamic decontamination of fresh-cut produce

Suneha Shukla[1], Manisha Shinde[2], Ajinkya Lade[2], Shweta Jagtap[3], Sandeep Pai[4], Garima Gupta[1*], Surekha Satpute[2], Umesh Jadhav[2*]

[1]Faculty of Biosciences, Institute of Biosciences and Technology, Shri Ramswaroop Memorial University, Barabanki, India.
[2]Department of Microbiology, Savitribai Phule Pune University, Pune, India.
[3]Department of Instrumentation Science, Savitribai Phule Pune University, Pune, India.
[4]Department of Botany, Rayat Shikshan Sanstha's Dada Patil Mahavidyalaya, Karjat, India.

ARTICLE INFO

Article history:
Received on: 17/02/2026
Accepted on: 26/06/2026
Available Online: 25/09/2026

Key words:
Fresh-cut produce, *Salmonella typhimurium*, chlorophyllin–$Ca_3(PO_4)_2$ nanohybrid, photodynamic decontamination, food safety

ABSTRACT

Photodynamic decontamination using chlorophyllin is often limited by photosensitizer leaching, surface staining, poor reusability, and inconsistent antimicrobial performance. To address these challenges, a food-compatible chlorophyllin–$Ca_3(PO_4)_2$ nanohybrid was synthesized and optimized to improve chlorophyllin immobilization and photodynamic efficacy. Encapsulation efficiency increased with calcium ion concentration and incubation time, reaching approximately 99% under optimized synthesis conditions despite the absence of highly ordered nanoflower architectures. Upon visible-light irradiation, the nanohybrid exhibited potent antibacterial activity against *Salmonella typhimurium*, achieving approximately 98% bacterial reduction. Additional studies demonstrated effective photodynamic inactivation (PDI) of gram-positive bacteria, including *Staphylococcus aureus* and *Bacillus subtilis*, confirming broad-spectrum antimicrobial activity. Reactive oxygen species scavenger assays identified singlet oxygen as the primary antimicrobial species responsible for bacterial inactivation, while fluorescence staining, scanning electron microscopy analysis, and intracellular leakage studies confirmed extensive membrane disruption. The nanohybrid also achieved approximately 98% PDI of naturally occurring microbial populations recovered from fresh-cut cucumber, cabbage, and spinach surfaces. Unlike free chlorophyllin, the immobilized nanohybrid showed negligible chlorophyllin release, no visible surface staining, and retained substantial antibacterial activity over multiple reuse cycles. Collectively, these findings demonstrate that chlorophyllin–$Ca_3(PO_4)_2$ nanohybrid provides a reusable, non-migrating, and consumer-compatible photodynamic platform for enhancing the microbial safety of fresh-cut produce.

1. INTRODUCTION

Fresh-cut produce (FCP) is widely consumed because it is rich in bioactive phytochemicals, vitamins, minerals, and other health-promoting secondary metabolites [1]. However, the minimal processing involved in its preparation and its frequent consumption in raw form make FCP highly vulnerable to microbial contamination and subsequent spoilage [2]. Numerous foodborne disease outbreaks worldwide have been linked to contaminated fresh fruits and vegetables, with *Escherichia coli* and *Salmonella* among the most frequently implicated pathogens [3]. According to the World Health Organization, foodborne and waterborne diseases continue to pose a significant global public health burden, highlighting the urgent need for effective and sustainable food safety interventions [4].

Conventional decontamination approaches for FCP include physical treatments such as ultraviolet irradiation, high-pressure processing, ultrasound, and pulsed electric fields, as well as chemical sanitizers [5]. Although these methods can reduce microbial contamination, their effectiveness is often limited under industrial conditions, and some treatments may adversely affect the sensory and nutritional quality of produce or require substantial energy input. Chlorine-based sanitizers remain the most widely used decontamination agents; however, their application is associated with the formation of potentially toxic and carcinogenic disinfection by-products [6]. These limitations have stimulated interest in alternative non-thermal, environmentally friendly technologies for fresh-produce decontamination.

Nanotechnology has emerged as a promising platform for microbial control owing to its high efficiency, tunable physicochemical properties, and multifunctionality [7]. In particular, light-activated antimicrobial approaches, including photodynamic and photothermal treatments, have demonstrated considerable potential for pathogen inactivation

*Corresponding Author
Umesh Jadhav, Department of Microbiology, Savitribai Phule Pune University, Pune, India. E-mail: umeshjadhav02 @ gmail.com and

Garima Gupta, Faculty of Biosciences, Institute of Biosciences and Technology, Shri Ramswaroop Memorial University, Barabanki, India. E-mail: garimagupta.ibst@srmu.ac.in

© 2026 Suneha Shukla *et al.* This is an open access article distributed under the terms of the Creative Commons Attribution License -NonCommercial-ShareAlike Unported License (http://creativecommons.org/licenses/by-nc-sa/3.0/).

without contributing to antimicrobial resistance [8]. Photodynamic inactivation (PDI) relies on photosensitizers that generate reactive oxygen species (ROS) upon light irradiation, resulting in irreversible oxidative damage to microbial membranes, proteins, and nucleic acids [7]. Among the available photosensitizers, chlorophyll derivatives have attracted considerable attention because of their natural origin, abundance, and food-grade status. Chlorophyllin, a water-soluble semi-synthetic derivative of chlorophyll, efficiently generates ROS under visible light and has been successfully applied for microbial inactivation on food surfaces [9]. Several studies have demonstrated effective photodynamic decontamination of fruits, vegetables, and food-contact surfaces using chlorophyllin-based systems without compromising product quality [10].

Despite these advantages, free chlorophyllin suffers from several limitations, including photobleaching, photosensitizer leaching, surface staining, and poor reusability, which restrict its practical application. Recent advances in organic–inorganic nanohybrid and nanoflowers, hierarchical nanostructures characterized by high surface area and enhanced structural stability, offer promising opportunities to overcome these challenges [11,12]. Immobilization of bioactive molecules within such a nanohybrid has been shown to improve functional stability, catalytic performance, and reusability [13]. Notably, plant-derived biomolecules have also been successfully incorporated into nanohybrid structures, replacing proteins or enzymes as organic building blocks [14,15].

Recent advances in antimicrobial PDI have increasingly focused on the development of nanostructured carrier systems to improve photosensitizer stability, loading capacity, controlled delivery, and ROS generation efficiency. Among these, metal–organic frameworks (MOFs), MOF-derived nanozymes, photoresponsive hydrogels, and multifunctional nanocomposites have emerged as promising platforms for antimicrobial phototherapy due to their high surface area, tunable porosity, and versatile surface chemistry [16–19]. Recent studies have demonstrated the successful application of MOF-based systems for photosensitizer encapsulation, biofilm eradication, infected wound treatment, and synergistic photodynamic–photothermal or photodynamic–antibiotic therapies through enhanced ROS generation and controlled delivery of photoactive agents [20–22]. Despite their promising performance, many MOF-based systems rely on multistep synthesis procedures, specialized organic ligands, organic solvents, solvothermal processing, and relatively complex fabrication strategies that may increase production costs and limit large-scale implementation [19,22]. Consequently, there remains a need for simpler, environmentally benign, and scalable photosensitizer delivery platforms that can maintain high photodynamic efficiency while reducing material and processing complexity, particularly for food safety applications where practical implementation and regulatory acceptance are important considerations.

Calcium phosphate-based nanomaterials represent an attractive alternative owing to their low toxicity, biodegradability, environmental compatibility, and ease of preparation under mild aqueous conditions. In contrast to many advanced nanocarrier systems, calcium phosphate nanohybrid can be synthesized using inexpensive precursors without the need for harsh reaction conditions, toxic organic solvents, high-temperature solvothermal treatments, or elaborate surface modifications. Furthermore, calcium phosphate materials are capable of interacting with and stabilizing a wide range of bioactive compounds, making them promising carriers for naturally derived photosensitizers [23,24]. These characteristics are particularly advantageous for food safety applications, where simple, sustainable, and scalable antimicrobial technologies are required for the decontamination of fresh-cut fruits and vegetables. Incorporation of chlorophyllin, a water-soluble derivative of chlorophyll with well-established photosensitizing properties, into a calcium phosphate matrix may therefore provide an environmentally friendly and effective strategy for photodynamic microbial control.

In this study, we report the synthesis, optimization, and application of a food-compatible chlorophyllin–$Ca_3(PO_4)_2$ nanohybrid for light-triggered antimicrobial decontamination of FCP. The work focuses on improving chlorophyllin immobilization, enhancing photodynamic antibacterial efficacy, minimizing photosensitizer migration, and enabling material reusability. By combining a food-grade photosensitizer with a simple, aqueous-based calcium phosphate nanohybrid platform, this study offers a sustainable and consumer-friendly alternative to conventional chemical sanitizers for fresh-produce decontamination.

2. MATERIALS AND METHODS

2.1. Materials

Chlorophyllin sodium salt and the reagents used for phosphate-buffered saline (PBS) preparation were obtained from Sigma–Aldrich (Catalog No. 8048-12-6). *Luria–Bertani* (LB) broth and *Mueller–Hinton* agar were purchased from HiMedia Laboratories Pvt. Ltd., India (Catalog Nos. M001 and M173, respectively) and were used for bacterial cultivation and viable count determination.

2.2. Methods

2.2.1. Synthesis of $Ca_3(PO_4)_2$-nanohybrid with and without chlorophyllin

Chlorophyllin sodium salt was used as the organic component for nanohybrid synthesis. $Ca_3(PO_4)_2$ nanohybrids were prepared in the presence and absence of chlorophyllin to evaluate the effect of photosensitizer incorporation. Briefly, 1 ml of $CaCl_2$ stock solution (200 mM) and 200 µl of chlorophyllin stock solution (25 mM, unless otherwise specified) were added to 100 ml (PBS; 10 mM, pH 7.4). The reaction mixtures were vortexed for 30 seconds and incubated at 4°C in the dark for 72 hours under static conditions. Following incubation, the resulting precipitates were recovered by centrifugation at 5,000 × g for 15 minutes, washed twice with PBS to remove unbound components, and dried at 4°C in the dark to obtain the nanohybrid powder. Control $Ca_3(PO_4)_2$ nanohybrids were synthesized under identical conditions in the absence of chlorophyllin, with all other reaction parameters maintained unchanged.

2.2.2. Characterization of nanohybrid

The structural and morphological characteristics of the synthesized nanohybrids were investigated using complementary analytical techniques. Surface morphology was examined by scanning electron microscopy (SEM; FEI Nova NanoSEM 450; resolution 1 nm at 15 kV and 30 Pa) at the Central Instrumentation Facility, Savitribai Phule Pune University. Chlorophyllin incorporation into the calcium phosphate matrix was confirmed by Fourier transform infrared spectroscopy (Bruker Platinum Tensor 37). Crystalline phase analysis was performed using X-ray diffraction (XRD) on a PANalytical Empyrean-4 diffractometer.

2.2.3. Optimization of nanohybrid synthesis

Chlorophyllin-loaded nanohybrids were synthesized by systematically varying the $CaCl_2$ stock solution concentration, chlorophyllin

concentration, PBS volume, incubation temperature, and incubation time. To evaluate the effect of calcium concentration, 1 ml of $CaCl_2$ stock solution (100–700 mM) was added to 100 ml PBS (10 mM, pH 7.4) together with 200 µl of chlorophyllin stock solution (25 mM), followed by incubation at 4°C for 72 hours. A control reaction containing PBS and chlorophyllin but lacking $CaCl_2$ was prepared under identical conditions. Following incubation, the precipitate and supernatant were separated by centrifugation at 5,000 × g for 15–20 minutes. The recovered precipitates were dried and subjected to SEM analysis. Encapsulation efficiency (EE) was determined by quantifying the concentration of unencapsulated chlorophyllin remaining in the supernatant after nanohybrid formation. Briefly, the absorbance of the supernatant was measured at 406 nm using a UV–visible spectrophotometer, and chlorophyllin concentration (mg ml^{-1}) was estimated from the corresponding absorbance values. The EE was subsequently calculated using Equation (1).

$$\textbf{Encapsulation Efficiency}\,(\%) = \left(\frac{C_0 - C_S}{C_0}\right) \times 100 \qquad (1)$$

where:

C_0 = initial chlorophyllin concentration before nanohybrid synthesis (mg ml^{-1})

C_S = concentration of unencapsulated chlorophyllin in the supernatant (mg ml^{-1}).

To investigate the effect of buffer volume on nanohybrid formation, the PBS volume was varied from 10 to 100 ml while maintaining constant additions of 1-ml $CaCl_2$ stock solution (200 mM) and 200-µl chlorophyllin stock solution (25 mM). The reaction mixtures were incubated under the standard synthesis conditions described above, and the resulting precipitates were recovered by centrifugation for further analysis. Only the PBS volume was varied during this experiment; therefore, the final reagent concentrations changed proportionally with the reaction volume.

The influence of chlorophyllin concentration on nanohybrid formation and EE was evaluated by varying the chlorophyllin stock solution concentration from 5 to 25 mM while maintaining constant reaction conditions comprising 100-ml PBS (10 mM) and 1 ml of 200 mM $CaCl_2$ stock solution. Following incubation, the precipitate and supernatant fractions were separated by centrifugation and analyzed to determine EE.

To assess the effect of incubation temperature, reaction mixtures containing 100-ml PBS (10 mM), 1 ml of 200-mM $CaCl_2$ stock solution, and 200 µl of 25 mM chlorophyllin stock solution were incubated either at 4°C or at room temperature (30°C) under otherwise identical conditions. The effect of incubation time on chlorophyllin encapsulation was investigated by incubating identical reaction mixtures for 24, 48, and 72 hours. At each designated time point, the precipitate and supernatant were separated by centrifugation and subsequently analyzed.

2.2.4. Photodynamic antibacterial activity assay

The antibacterial activity of chlorophyllin was evaluated against *Salmonella typhimurium* NCIM 2501 (*S. typhimurium*) using a direct-contact PDI assay. The bacterial culture was grown in LB broth at 37°C under aerobic conditions and harvested by centrifugation at 5,000 × g for 15 minutes. The resulting cell pellet was washed and resuspended in sterile distilled water, and the bacterial suspension was adjusted to an optical density of OD_{600} = 0.1. For the photodynamic treatment, 900-µl aliquots of the standardized bacterial suspension were transferred to sterile microcentrifuge tubes and mixed with chlorophyllin solution at the desired concentration. The photokilling activity was initiated by exposing the reaction mixture, held in transparent glass bottles, to a cool white LED bulb (20 W, 6500 K; broad visible spectrum emission). The light source was positioned at a fixed distance of 4.5 cm from the sample surface, and illumination was carried out for 25 minutes under identical experimental conditions for all treatments. The irradiance at the sample position was estimated using a smartphone-based light meter application (light meter, Android platform) and was found to be 412.7 ± 3.1 W/m² [mean ± standard deviation (SD), n = 3]. Based on the irradiation time, the corresponding estimated fluence dose was approximately 74.3 J/cm². Following illumination, the samples were serially diluted in sterile saline solution, and 10-µl aliquots of appropriate dilutions were spread onto *Mueller–Hinton* agar plates. The plates were incubated at 37°C for 24 hours, after which viable bacterial colonies were enumerated and expressed as colony-forming units (CFU). To compare the antibacterial performance of the immobilized and free photosensitizer systems, a parallel experiment was performed using chlorophyllin–$Ca_3(PO_4)_2$ nanohybrid (10 mg) instead of free chlorophyllin while maintaining identical bacterial concentrations, illumination conditions, and incubation parameters. Antibacterial efficacy was expressed as log reduction and percentage reduction in viable bacterial counts, calculated according to Equations (2) and (3).

$$\textbf{Log Reduction} = \log_{10}\left(\frac{N_0}{N}\right) \qquad (2)$$

where:

N_0 = microbial count of untreated control (CFU ml^{-1})

N = microbial count after treatment (CFU ml^{-1}).

$$\textbf{Percentage Reduction}\,(\%) = \left(\frac{N_0 - N}{N}\right) \times 100 \qquad (3)$$

where:

N_0 = microbial count of untreated control (CFU ml^{-1})

N = microbial count after treatment (CFU ml^{-1}).

A decrease in CFU/ml relative to untreated controls was considered indicative of antimicrobial activity.

2.2.5. Evaluation of photodynamic antibacterial activity against gram-positive bacteria

To evaluate the antibacterial spectrum of the chlorophyllin–$Ca_3(PO_4)_2$ nanohybrid beyond gram-negative bacteria, PDI studies were performed against *Staphylococcus aureus* NCIM 5021 and *Bacillus subtilis* NCIM 2724. Bacterial cultures were prepared as described in Section "Photodynamic antibacterial activity assay". Briefly, 990-µl aliquots of bacterial suspension (OD_{600} = 0.1) were mixed with the chlorophyllin–$Ca_3(PO_4)_2$ nanohybrid and subjected to photodynamic treatment under the optimized conditions described previously. Untreated control samples were maintained under identical conditions without the addition of the nanohybrid. Following treatment, viable bacterial counts were determined by serial dilution and plating

on *Mueller–Hinton* agar. Antibacterial efficacy was expressed as log reduction and percentage reduction in viable bacterial counts, calculated according to Equations (2) and (3). All experiments were performed in triplicate, and the results are presented as mean ± SD.

2.2.6. Effect of chlorophyllin concentration, light exposure time, and bacterial cell density on PDI

Salmonella typhimurium cultures were prepared as described previously. To optimize the photodynamic treatment conditions, the effects of chlorophyllin concentration (5–25 mM), illumination time (5–30 minutes), and initial bacterial cell density (OD_{600} = 0.1–0.3) were systematically evaluated. For each experiment, a single parameter was varied while all other conditions were maintained constant. Following treatment, antibacterial activity was determined by viable colony counting as described earlier and expressed as CFU, log reduction, and percentage reduction.

2.2.7. Effect of nanohybrid amount, light exposure time, and bacterial cell density on nanohybrid-mediated PDI

The photodynamic antibacterial activity of the chlorophyllin–$Ca_3(PO_4)_2$ nanohybrid against *S. typhimurium* was evaluated using the procedure described above. To optimize treatment conditions, the effects of nanohybrid dosage (5–15 mg), illumination time, and initial bacterial cell density (OD_{600}= 0.1–0.3) were systematically investigated by varying one parameter at a time while maintaining all other conditions constant. Antibacterial efficacy was determined by viable colony enumeration following serial dilution and plating, and the results were expressed as CFU, log reduction, and percentage reduction in bacterial counts.

2.2.8 ROS scavenger assay

The involvement of ROS in the photodynamic antibacterial activity of the chlorophyllin–$Ca_3(PO_4)_2$ nanohybrid was investigated using selective ROS scavengers, following methodologies commonly employed in antimicrobial PDI studies [25–27]. Sodium azide and mannitol were selected as scavengers of singlet oxygen ($^1O_2$) and hydroxyl radicals (•OH), respectively, because of their well-established ROS-quenching properties [28]. *Salmonella typhimurium* was cultivated in LB broth at 37°C until the exponential growth phase was reached. Cells were harvested by centrifugation at 10,000 × g for 10 minutes, washed twice with sterile distilled water, and resuspended in sterile distilled water. The bacterial suspension was adjusted to an optical density of OD_{600} = 0.1. For each treatment, 900 µl of the standardized bacterial suspension was transferred to sterile microcentrifuge tubes and supplemented with 10 mg of chlorophyllin–$Ca_3(PO_4)_2$ nanohybrid.

To evaluate the contribution of individual ROS species, either sodium azide (100-mM stock solution; 10 µl) or mannitol (1-M stock solution; 10 µl) was added prior to illumination, resulting in final concentrations of approximately 1 and 10 mM, respectively. The lower concentration of sodium azide was selected because of its high efficiency as a singlet oxygen quencher, whereas the higher concentration of mannitol was employed to compensate for its comparatively lower hydroxyl radical scavenging capacity [25,27]. Control samples consisted of bacterial suspensions supplemented with sterile distilled water to maintain the same final reaction volume as the treatment groups. Photodynamic reactions were initiated immediately by exposure to visible-light irradiation under the optimized conditions described previously. Following 25 minutes of illumination, the samples were serially diluted in sterile saline solution and spread plated onto *Mueller–Hinton* agar. After incubation at 37°C for 24 hours, viable colonies were enumerated and expressed as CFU. Antibacterial efficacy was calculated as log reduction and percentage reduction in viable bacterial counts according to Equations (2) and (3). All experiments were performed in triplicate, and the results are presented as mean ± SD.

2.2.9. Live–dead cell staining of S. typhimurium treated with chlorophyllin–$Ca_3(PO_4)_2$ nanohybrid

The effect of chlorophyllin–$Ca_3(PO_4)_2$ nanohybrid on bacterial viability and membrane integrity was evaluated using acridine orange/ethidium bromide (AO/EtBr) dual fluorescence staining. *Salmonella typhimurium* cultures were prepared and subjected to photodynamic treatment under the optimized conditions described previously. Following treatment, bacterial cells were harvested by centrifugation at 5,000 × g for 10 minutes, washed twice with sterile saline, and resuspended in a staining solution containing AO/EtBr (1 µg ml^{-1} each). After incubation in the dark at room temperature for 30 minutes, the cells were washed twice with sterile saline and resuspended in sterile saline.

For fluorescence microscopy, stained cell suspensions were mixed with an equal volume of 0.8% agarose, and 10-µl aliquots were mounted on glass slides. Samples were examined using a Zeiss Axioscope A1 fluorescence microscope under a 100× objective with excitation and emission filters of 495 and 515 nm, respectively [29]. Viable cells with intact membranes exhibited green fluorescence due to AO uptake, whereas membrane-compromised or dead cells exhibited red fluorescence as a result of ethidium bromide penetration and nucleic acid binding.

To obtain semi-quantitative validation of the fluorescence microscopy observations, AO and EtBr fluorescence intensities were additionally measured using a multimode microplate reader. Following photodynamic treatment, bacterial suspensions were serially diluted in sterile saline, and appropriate dilutions were transferred to black 96-well microplates in triplicate. AO (5 µl, 100 µg ml^{-1}) and ethidium bromide (5 µl, 100 µg ml^{-1}) were added to each well, followed by incubation in the dark for 15 minutes at room temperature. AO fluorescence was recorded at excitation/emission wavelengths of 485/530 nm, whereas EtBr fluorescence was measured at 530/620 nm. Blank wells containing AO and EtBr in saline without bacterial cells were used for background correction. Corrected fluorescence intensities, fluorescence ratios, and viability parameters were calculated according to Equations (4)–(8).

$$\textbf{Corrected AO} = \textbf{AO}_{\textbf{Sample}} - \textbf{AO}_{\textbf{Blank}} \quad (4)$$

$$\textbf{Corrected EtBr} = \textbf{EtBr}_{\textbf{Sample}} - \textbf{EtBr}_{\textbf{Blank}} \quad (5)$$

The red/green fluorescence ratio, used as an indicator of bacterial membrane damage and cell viability, was calculated as follows:

$$\textbf{Fluorescence Ratio} = \frac{\mathbf{F_{EtBr}}}{\mathbf{F_{AO}}} \quad (6)$$

where:

F_{EtBr} = corrected EtBr fluorescence intensity

F_{AO} = corrected AO fluorescence intensity.

The percentage of live and dead bacterial cells was calculated according to the following equations:

Live cell percentage,

$$\text{Live Cells}\,(\%) = \frac{F_{AO}}{F_{AO} + F_{EtBr}} \times 100 \quad (7)$$

where:

F_{EtBr} = corrected EtBr fluorescence intensity

F_{AO} = corrected AO fluorescence intensity.

Dead cell percentage,

$$\text{Dead Cells}\,(\%) = \frac{F_{EtBr}}{F_{AO} + F_{EtBr}} \times 100 \quad (8)$$

where:

F_{EtBr} = corrected EtBr fluorescence intensity

F_{AO} = corrected AO fluorescence intensity.

All fluorescence measurements were performed in triplicate (n = 3), and results are expressed as mean ± SD.

The AO/EtBr fluorescence-based viability analysis was performed with minor modifications based on previously reported ratiometric fluorescence methods for rapid bacterial viability quantification.

2.2.10. Mechanistic investigation of photoactive killing of S. typhimurium by chlorophyllin–$Ca_3(PO_4)_2$ nanohybrid

Field-emission scanning electron microscopy (FESEM; Quanta FEG 450, the Netherlands) was used to examine morphological alterations in *S. typhimurium* cells following photodynamic treatment, as described previously [30] with minor modifications. Briefly, treated bacterial cells were washed with PBS, fixed with 2.5% (v/v) glutaraldehyde at 4°C overnight, and subsequently dehydrated through a graded ethanol series (20%, 40%, 60%, 80%, and 90%) for 15 minutes each, followed by two washes with absolute ethanol. A 2-µl aliquot of the dehydrated cell suspension was air-dried, sputter-coated with gold, and examined by FESEM.

Membrane integrity was further evaluated by determining the leakage of intracellular constituents, as described previously [31]. Following photodynamic treatment, the bacterial suspensions were centrifuged, and the resulting supernatants were analyzed spectrophotometrically at 260 and 280 nm. Absorbance at 260 and 280 nm was used as an indicator of extracellular nucleic acids and proteins, respectively, released as a consequence of membrane damage.

2.2.11. Decontamination of FCP using chlorophyllin solution and chlorophyllin–$Ca_3(PO_4)_2$ nanohybrid

The antibacterial efficacy of free chlorophyllin and chlorophyllin–$Ca_3(PO_4)_2$ nanohybrid for FCP decontamination was evaluated using cucumber slices as a model system. Fresh cucumbers were sliced aseptically and surface-sterilized by immersion in 70% ethanol, followed by thorough rinsing with sterile distilled water to remove residual ethanol.

Artificial contamination was achieved by uniformly spreading 100 µl of a *S. typhimurium* suspension (OD_{600} = 0.1) onto the surface of each cucumber slice. The inoculated slices were maintained at room temperature for 30 minutes to facilitate bacterial attachment and subsequently air-dried. The contaminated slices were then divided into two treatment groups: (i) free chlorophyllin (25 mM) and (ii) chlorophyllin–$Ca_3(PO_4)_2$ nanohybrid. Following visible-light irradiation under the optimized photodynamic treatment conditions, the cucumber slices were washed with sterile saline, and the wash solutions were collected for microbiological analysis. Decontamination efficacy was determined by viable colony enumeration as described previously.

To further assess the practical applicability of the photodynamic system, additional experiments were performed using naturally occurring microflora recovered from cucumber, cabbage, and spinach surfaces, as described in Section "Assessment of PDI of natural produce-associated microflora".

2.2.12. Assessment of PDI of natural produce-associated microflora

To evaluate the effectiveness of the chlorophyllin–$Ca_3(PO_4)_2$ nanohybrid against naturally occurring microbial populations present on fresh produce surfaces, cucumber, cabbage, and spinach samples were examined without artificial inoculation. For cucumber, representative portions of the fruit were used, whereas approximately 8 × 8 cm sections of cabbage leaves and whole spinach leaves, including stem portions, were selected as representative leafy vegetables. The samples were immersed in sterile 10-mM PBS and incubated for 30 minutes to facilitate the release of surface-associated microorganisms into the buffer. Subsequently, 990 µl of the resulting microbial suspension was transferred to sterile microcentrifuge tubes and mixed with 10 mg of chlorophyllin–$Ca_3(PO_4)_2$ nanohybrid. The reaction mixtures were exposed to visible light under the optimized photodynamic treatment conditions described previously. Control samples received sterile distilled water in place of the nanohybrid while maintaining identical experimental conditions. Following treatment, microbial populations were quantified by viable colony enumeration as described earlier. Antimicrobial efficacy was expressed as log reduction and percentage reduction in microbial counts according to Equations (2) and (3). All experiments were performed in triplicate, and the results are presented as mean ± SD.

2.2.13. Evaluation of chlorophyllin retention and stability in the $Ca_3(PO_4)_2$ nanohybrid

The retention and stability of chlorophyllin immobilized within the chlorophyllin–$Ca_3(PO_4)_2$ nanohybrid were evaluated by monitoring chlorophyllin detected in the surrounding aqueous phase during prolonged exposure to PBS. Briefly, 10 mg of nanohybrid powder was suspended in 900 µl of PBS (pH 7.4) and incubated at room temperature. At predetermined time intervals (24, 48, 72, 96, and 120 hours), the suspension was centrifuged at 8,000 × g for 5 minutes, and the absorbance of the supernatant was measured at 405 nm using a UV–visible spectrophotometer. The absorbance values were used as an indicator of chlorophyllin present in the aqueous phase. Following each measurement, the pellet was resuspended in fresh PBS and returned to the incubation conditions until the next sampling interval. The nanohybrid samples were stored at 4°C between measurements. Changes in absorbance over time were used to assess the extent of chlorophyllin retention within the nanohybrid matrix and the stability of chlorophyllin immobilization under aqueous conditions.

2.2.14. Reusability of chlorophyllin–$Ca_3(PO_4)_2$ nanohybrid for photodynamic antibacterial activity

The reusability of the chlorophyllin–$Ca_3(PO_4)_2$ nanohybrid was evaluated over five consecutive PDI cycles against *S. typhimurium*. For the initial cycle, 10 mg of nanohybrid was suspended in 100 µl of sterile distilled water and mixed with 900 µl of bacterial suspension (OD_{600} = 0.1). Photodynamic treatment was performed under the optimized conditions described previously, while untreated controls received sterile distilled water instead of the nanohybrid. Following each treatment cycle, the nanohybrid particles were recovered by centrifugation at 5,000 × g for 10 minutes, resuspended in 100 µl of sterile distilled water, and reused with a fresh bacterial suspension for the subsequent cycle. This recovery and reuse procedure was repeated for five consecutive cycles under identical experimental conditions. Antibacterial efficacy after each cycle was determined by viable colony enumeration as described previously and expressed as CFU, log reduction, and percentage reduction relative to the untreated control. All experiments were performed in triplicate, and the results are presented as mean ± SD.

2.2.15. Statistical analysis

All experiments were performed in triplicate, and results are presented as mean ± SD. Statistical analysis was carried out using OriginPro software. Differences among treatment means were evaluated by one-way analysis of variance (ANOVA) according to the following model:

$$Yij = \mu + \tau i + \varepsilon ij$$

where Yij represents the observed value, μ is the overall mean, τi is the treatment effect, and εij is the random error. When significant differences were detected, Tukey's honestly significant difference test was applied for multiple comparisons. Differences were considered statistically significant at $p < 0.05$.

3. RESULTS AND DISCUSSION

3.1. Synthesis of Chlorophyllin–$Ca_3(PO_4)_2$ Nanohybrid

The successful synthesis of the chlorophyllin–$Ca_3(PO_4)_2$ nanohybrid demonstrates the feasibility of immobilizing a food-grade photosensitizer within an organic–inorganic matrix for photodynamic applications. Upon mixing chlorophyllin, $CaCl_2$, and PBS, the reaction mixture rapidly formed a fine green precipitate, indicating spontaneous nanohybrid formation. Such rapid precipitation is characteristic of organic–inorganic hybrid systems assembled through the interaction of metal ions and organic molecules in aqueous environments [32]. The formation of the nanohybrid is attributed to the interaction of Ca^{2+} ions with functional groups present in chlorophyllin, particularly carboxylate and hydroxyl moieties, which can serve as coordination sites and promote nucleation [33,34]. Simultaneously, phosphate ions present in PBS facilitate the formation of a calcium phosphate matrix, resulting in the co-assembly of chlorophyllin and inorganic calcium phosphate into a stable hybrid structure. The immediate appearance of the precipitate suggests that nanohybrid formation occurs spontaneously under mild aqueous conditions without the need for elevated temperatures, organic solvents, or additional cross-linking agents. Although the synthesized material did not exhibit a highly ordered flower-like architecture, subsequent characterization and functional studies confirmed effective chlorophyllin immobilization and photodynamic activity, indicating that functional performance was not dependent on the formation of a specific nanostructural morphology.

3.2. Morphological and Structural Characterization of Nanohybrid

The morphological features of $Ca_3(PO_4)_2$ and the chlorophyllin–$Ca_3(PO_4)_2$ nanohybrid were examined by SEM. Pure $Ca_3(PO_4)_2$ synthesized in the absence of chlorophyllin formed irregular, loosely aggregated precipitates (Fig. 3a). On the contrary, the chlorophyllin–$Ca_3(PO_4)_2$ nanohybrid exhibited aggregated and less-ordered morphologies rather than the highly organized flower-like architectures commonly reported for enzyme–inorganic nanoflowers (Fig. 3b; Supporting Document Fig. 1). These observations suggest isotropic calcium phosphate growth in the presence of chlorophyllin.

Despite the absence of a classical nanoflower morphology, the synthesized material exhibited high chlorophyllin EE and strong photodynamic antibacterial activity. In photodynamic systems, functional performance depends primarily on the accessibility and photoactivity of the immobilized photosensitizer rather than on the formation of a specific hierarchical structure. Although highly organized nanostructures may provide greater surface area and facilitate mass transfer, the antibacterial activity, ROS-scavenger studies, fluorescence staining, and intracellular leakage assays collectively demonstrate that chlorophyllin remained photoactive after immobilization within the calcium phosphate matrix. These findings indicate that effective nanohybrid formation is governed principally by molecular interactions between chlorophyllin and calcium phosphate rather than by the development of a particular morphology.

XRD analysis further confirmed nanohybrid formation (Fig. 4). Pure $Ca_3(PO_4)_2$ exhibited diffraction peaks characteristic of β-tricalcium phosphate (JCPDS 09-0169). Following chlorophyllin incorporation, the nanohybrid retained the characteristic calcium phosphate reflections, although with reduced intensity and noticeable peak broadening, indicating a decrease in long-range crystallinity. The absence of distinct chlorophyllin diffraction peaks suggests that chlorophyllin was molecularly dispersed or present in an amorphous state within the calcium phosphate matrix.

The broad diffraction features observed in the nanohybrid pattern further indicate that the calcium phosphate phase was predominantly amorphous, consistent with the formation of amorphous calcium phosphate (ACP). Compared with crystalline calcium phosphate phases, ACP typically possesses greater structural disorder and higher surface area, characteristics that may facilitate the incorporation and stabilization of bioactive molecules. In the present system, however, calcium phosphate primarily functioned as a support matrix, whereas chlorophyllin served as the photoactive component responsible for ROS generation under visible-light irradiation. Consequently, the observed antimicrobial activity is attributed principally to chlorophyllin-mediated ROS production rather than to the crystallinity of the calcium phosphate phase.

Because ROS generation and antibacterial activity were retained despite the largely amorphous nature of the support matrix, the present findings suggest that strict control over calcium phosphate crystallinity is not essential for achieving effective photodynamic performance. Nevertheless, comparative studies involving amorphous and crystalline calcium phosphate matrices, together with Brunauer-Emmett-Teller surface area analysis and direct ROS quantification, would provide valuable insight into the influence of structural organization on photosensitizer accessibility and photodynamic efficiency.

3.3. Optimization of Chlorophyllin EE

The efficiency of chlorophyllin immobilization was strongly influenced by calcium ion concentration (Fig. 1). Increasing the $CaCl_2$ stock solution concentration from 100 to 500 mM enhanced EE from 88.80% ± 0.71% to 98.76% ± 0.40%, indicating improved nucleation and greater incorporation of chlorophyllin within the developing calcium phosphate matrix. A further increase in $CaCl_2$ stock solution concentration resulted in a decline in EE, likely due to rapid bulk precipitation that reduced effective interactions between chlorophyllin molecules and the inorganic phase [35].

The volume of PBS also significantly affected nanohybrid formation. Maximum EE (98.73% ± 0.27%) was achieved at a PBS volume of 100 ml (Fig. 2), suggesting that increased reaction volume promoted more uniform ion distribution and controlled nucleation, thereby facilitating chlorophyllin incorporation. Similarly, chlorophyllin stock solution concentrations between 20 and 25 mM produced the highest EEs (Supporting Document Fig. 2), highlighting the importance of maintaining an appropriate balance between the organic and inorganic components during nanohybrid assembly.

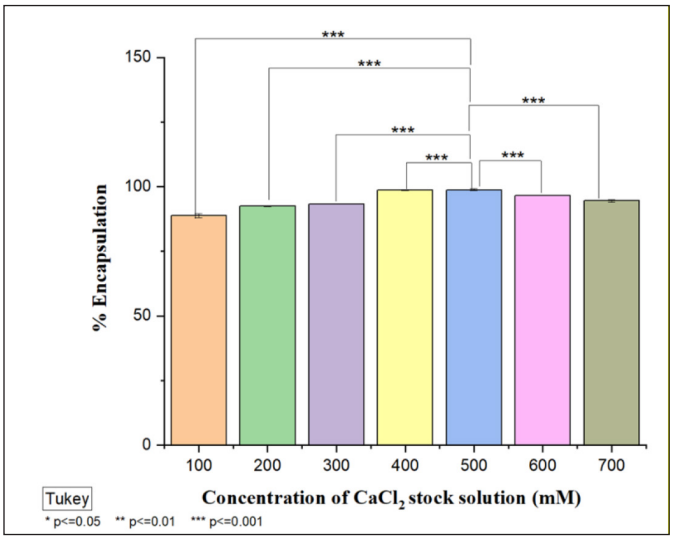

Figure 1. Effect of $CaCl_2$ stock solution concentration (100–700 mM; corresponding to final reaction concentrations of approximately 1–7 mM) on chlorophyllin EE.

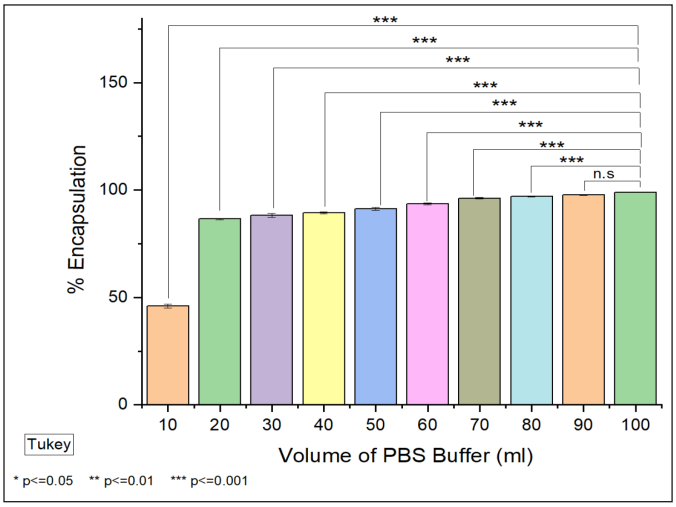

Figure 2. Effect of PBS buffer volume on chlorophyllin encapsulation.

On the contrary, incubation temperature exerted only a minor influence on chlorophyllin immobilization. However, incubation time markedly affected nanohybrid formation, with EE increasing from 79.19% ± 0.41% after 24 hours to 98.24% ± 0.18% after 72 hours (Supporting Document Fig. 3). The gradual increase observed over time suggests progressive incorporation and stabilization of chlorophyllin within the calcium phosphate matrix as nanohybrid growth proceeded.

Collectively, these results demonstrate that chlorophyllin immobilization is governed primarily by factors that influence calcium phosphate nucleation and growth. Under the optimized conditions identified in this study, near-complete encapsulation was achieved, providing a stable platform for subsequent photodynamic antimicrobial applications.

3.4. Photodynamic Antibacterial Activity of Free Chlorophyllin

The photodynamic antibacterial activity of free chlorophyllin was initially evaluated against *S. typhimurium* using a direct-contact photoinactivation assay. Increasing free chlorophyllin concentration from 5 to 25 mM progressively enhanced antibacterial activity, resulting in bacterial reductions ranging from approximately 37% to 99% (Supporting Document Figs. 4–7). Similarly, extending the illumination period from 5 to 30 minutes increased bacterial reduction from approximately 11% to 95%, confirming the importance of both photosensitizer concentration and light exposure for effective PDI. On the contrary, increasing the initial bacterial density (OD_{600} = 0.1–0.3) reduced antibacterial efficacy, with bacterial reduction decreasing from approximately 99% to 64%. This observation is consistent with the limited availability and diffusion range of ROS at higher cell densities, where a greater number of bacterial cells compete for the oxidative species generated during illumination. Collectively, these results confirm the photodynamic antibacterial potential of chlorophyllin against *S. typhimurium* and were used to identify the treatment conditions subsequently employed for evaluating the chlorophyllin–$Ca_3(PO_4)_2$ nanohybrid.

3.5. Photodynamic Antibacterial Activity of Chlorophyllin–$Ca_3(PO_4)_2$ Nanohybrid

The influence of operational parameters on chlorophyllin–$Ca_3(PO_4)_2$nanohybrid-mediated PDI of *S. typhimurium* was systematically evaluated. Increasing the initial bacterial density (OD_{600} = 0.1–0.3) resulted in a progressive decline in antibacterial efficacy, indicating that higher microbial loads reduce the effectiveness of photodynamic treatment under fixed illumination and nanohybrid amount (mg). Illumination time had a pronounced effect on bacterial inactivation. CFU reductions of approximately 9%, 38%, and 55% were observed after 5, 10, and 15 minutes of visible-light exposure, respectively, while approximately 98% bacterial reduction was achieved after 25 minutes. Statistical analysis revealed significant differences among illumination times, confirming that prolonged light exposure enhanced photodynamic antibacterial activity. The progressive increase in bacterial reduction with increasing illumination duration is consistent with the cumulative generation of ROS during treatment. Nanohybrid dosage also significantly influenced antibacterial performance. Increasing the nanohybrid amount enhanced bacterial inactivation, with 10 mg identified as the minimum dosage required to achieve near-maximal antibacterial activity under the optimized conditions. Tukey's post hoc analysis demonstrated significant differences between lower and higher nanohybrid

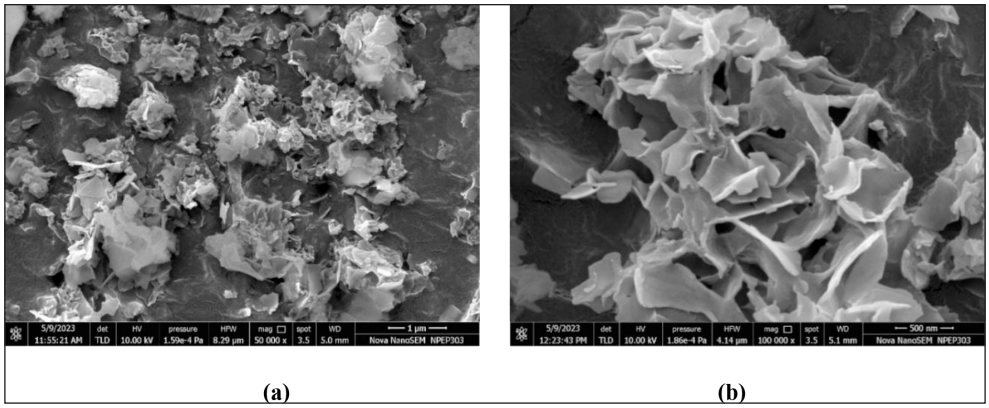

Figure 3. SEM showing morphology of synthesized nanohybrid. (a) $Ca_3(PO_4)_2$. (b) Chlorophyllin–$Ca_3(PO_4)_2$.

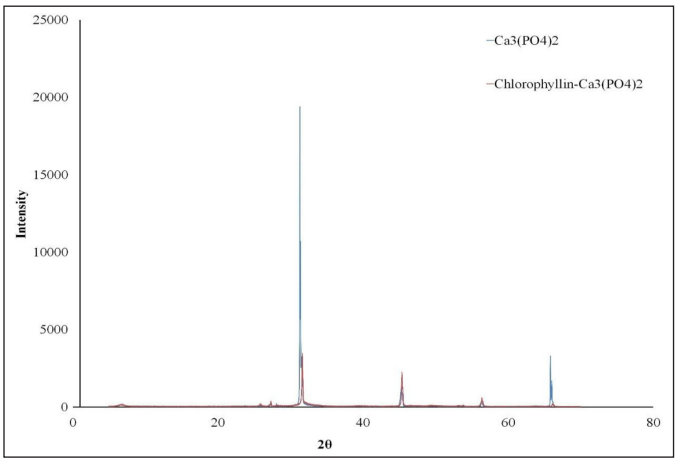

Figure 4. Comparative XRD profiles of $Ca_3(PO_4)_2$ and chlorophyllin–$Ca_3(PO_4)_2$.

Table 1. Antibacterial efficacy of chlorophyllin–$Ca_3(PO_4)_2$ nanohybrid against gram-positive bacterial strains following photodynamic treatment.

Bacteria	Log reduction (Mean ± STDEV)	Reduction (%) (Mean ± STDEV)
S. aureus	2.33 ± 0.18*	99.84 ± 0.23
Bacillus subtilis	2.40 ± 0.01	100.00

*For statistical calculation of log reduction, a detection limit of 1 CFU was assumed.

dosages, supporting the concentration-dependent enhancement of photodynamic efficacy. Although further increases in nanohybrid dosage produced only marginal improvements in bacterial reduction, this observation suggests that the system approached its maximum antibacterial performance under the experimental conditions employed (Supporting Document Fig. 8). Collectively, these results demonstrate that bacterial load, illumination time, and nanohybrid dosage are key determinants of photodynamic performance. The statistically significant improvements observed with increasing illumination time and nanohybrid dosage support the robustness of the optimized treatment conditions selected for subsequent experiments.

3.6. PDI of Gram-Positive Bacteria

To determine whether the antimicrobial activity of chlorophyllin–$Ca_3(PO_4)_2$ nanohybrid extends beyond gram-negative bacteria, PDI studies were conducted using the gram-positive organisms *S. aureus* and *B. subtilis*. These bacteria possess thick peptidoglycan cell walls and are often considered more challenging targets for antimicrobial agents due to structural differences compared with gram-negative organisms.

Photodynamic treatment of *S. aureus* reduced viable counts from 211.33 ± 3.50 CFU in untreated controls to 0.33 ± 0.52 CFU following visible-light activation of the nanohybrid. This corresponded to a mean log reduction of 2.33 ± 0.18 log CFU and a percentage reduction of 99.84% ± 0.23% (Table 1). Similarly, treatment of *B. subtilis* resulted in the complete elimination of detectable colonies, reducing viable counts from 250.33 ± 7.77 CFU in the untreated control to zero detectable colonies after treatment. This corresponded to a mean log reduction of 2.40 ± 0.01 log CFU and complete (100%) bacterial inactivation (Table 1).

The observed activity against both gram-positive species demonstrates that the photodynamic antimicrobial action of chlorophyllin–$Ca_3(PO_4)_2$ nanohybrid is not restricted to gram-negative bacteria such as *S. typhimurium*. Upon visible-light irradiation, chlorophyllin generates ROS, including singlet oxygen and free radicals, which can rapidly oxidize membrane lipids, proteins, and nucleic acids. Because ROS-mediated damage targets multiple cellular components simultaneously, bacterial susceptibility is less dependent on classical antibiotic-resistance mechanisms.

Particularly noteworthy was the complete elimination of detectable *B. subtilis* cells following treatment, indicating highly effective ROS-mediated killing even in gram-positive organisms possessing robust peptidoglycan layers. Together with the previously observed activity against *S. typhimurium*, these results demonstrate the broad-spectrum antibacterial efficacy of the chlorophyllin–$Ca_3(PO_4)_2$ nanohybrid and support their potential application as a versatile photodynamic antimicrobial platform for food-safety applications.

3.7. Comparative Photodynamic Antibacterial Efficacy of Free Chlorophyllin and Chlorophyllin–$Ca_3(PO_4)_2$ Nanohybrid

The photodynamic antibacterial activity of the chlorophyllin–$Ca_3(PO_4)_2$ nanohybrid was evaluated and compared with free chlorophyllin. Untreated controls, light-only controls, and nanohybrid-only controls exhibited negligible reductions in viable bacterial counts, confirming that neither visible light nor the nanohybrid alone possessed significant antibacterial activity under the experimental conditions. On the contrary, visible-light irradiation in the presence of the nanohybrid resulted in substantial inactivation of *S. typhimurium*.

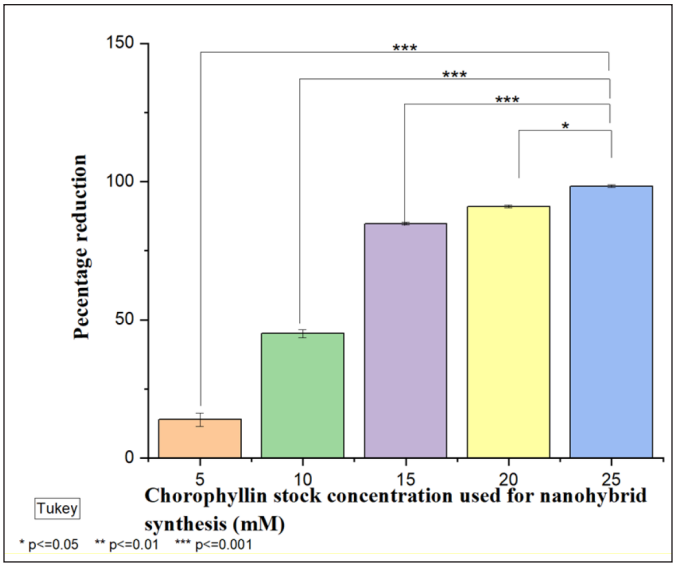

Figure 5. Effect of chlorophyllin stock solution concentration (5–25 mM) used during nanohybrid synthesis on the PDI of *S. typhimurium* by the chlorophyllin–$Ca_3(PO_4)_2$ nanohybrid.

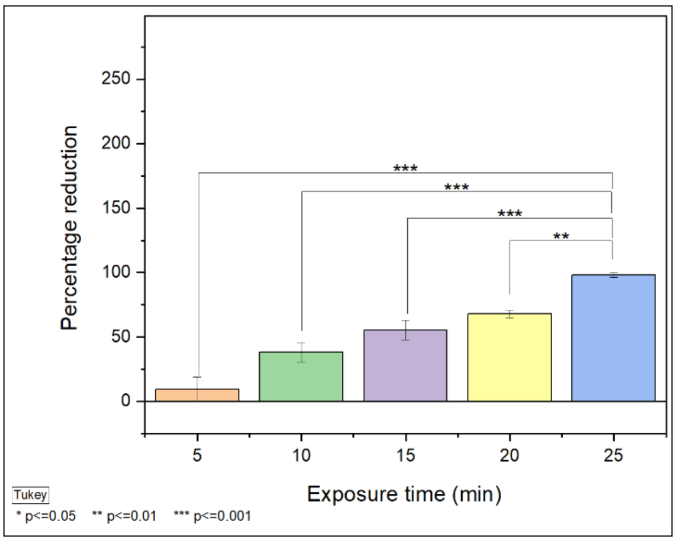

Figure 6. Effect of exposure time on the photokilling of *S. typhimurium* using chlorophyllin–$Ca_3(PO_4)_2$ nanohybrid.

Nanohybrids synthesized using increasing chlorophyllin loading during nanohybrid synthesis (stock concentration, mM) exhibited progressively greater antibacterial activity (Fig. 5). The percentage reduction increased from 13.90% ± 4.20% at 5 mM to 98.83% ± 0.30% at 25 mM, indicating that higher chlorophyllin loading enhanced photodynamic efficacy. One-way ANOVA followed by Tukey's multiple comparison test confirmed significant differences between most treatment levels. Significant increases in antibacterial activity were observed between 5 and 10, 10 and 15, and 15 and 25-mM nanohybrids ($p < 0.001$). Although the increase between 15 and 20 mM was less pronounced, it remained statistically significant ($p < 0.05$). These findings demonstrate that increasing chlorophyllin incorporation within the nanohybrid significantly improves antibacterial performance, likely by increasing the number of photoactive sites available for ROS generation under visible-light irradiation.

Photosensitizers are often less effective against gram-negative bacteria because the negatively charged outer membrane can restrict photosensitizer interaction and partially protect cells from oxidative damage [9,36,37]. Nevertheless, the chlorophyllin–$Ca_3(PO_4)_2$ nanohybrid achieved efficient inactivation of *S. typhimurium* under visible-light exposure.

Illumination time also exerted a significant influence on antibacterial activity (Fig. 6). The percentage reduction increased from 9.28% ± 9.59% after 5 minutes of illumination to 98.16% ± 1.59% after 25 minutes. Tukey's multiple comparison analysis revealed significant differences between 5 and 10 minutes ($p < 0.01$), 5 and 15 minutes ($p < 0.001$), and 5 and 20 minutes ($p < 0.001$). On the contrary, differences between 10 and 15 minutes and between 15 and 20 minutes were not statistically significant ($p > 0.05$), suggesting a more gradual increase in antibacterial activity during the intermediate stages of treatment. However, 25 minutes of illumination produced significantly greater bacterial inactivation than all shorter exposure periods ($p < 0.001$), resulting in near-complete inactivation. These results confirm that photodynamic efficacy is strongly dependent on irradiation time and support the role of cumulative ROS generation during prolonged visible-light exposure.

The enhanced antibacterial performance of the nanohybrid compared with free chlorophyllin is attributed to immobilization of chlorophyllin within the calcium phosphate matrix, which promotes close association between photoactive sites and bacterial cells. Because ROS possess short lifetimes and limited diffusion distances, localized ROS generation at or near the bacterial surface is expected to enhance oxidative damage to cellular membranes and improve antibacterial efficiency. This interpretation is consistent with the ROS-scavenger experiments, fluorescence staining, SEM observations, and intracellular leakage studies presented in subsequent sections.

3.8. ROS-Mediated Antibacterial Mechanism

To identify the ROS responsible for bacterial inactivation, photodynamic antibacterial assays were performed in the presence of sodium azide and mannitol, which selectively quench singlet oxygen ($^1O_2$) and hydroxyl radicals (•OH), respectively. ROS-scavenger experiments are widely employed to elucidate the mechanisms underlying antimicrobial PDI [25,26].

In the presence of mannitol, viable *S. typhimurium* counts decreased from 218.00 ± 12.96 CFU in the untreated control to 7.67 ± 1.21 CFU following photodynamic treatment, corresponding to a log reduction of 1.46 ± 0.08 and a percentage reduction of 96.47% ± 0.60% (Table 2). Although antibacterial activity remained substantial, the slight decrease in efficacy compared with the scavenger-free treatment suggests that hydroxyl radicals may contribute to bacterial killing but are unlikely to be the dominant ROS species involved. On the contrary, the addition of sodium azide almost completely suppressed antibacterial activity, with viable counts remaining at 197.67 ± 2.16 CFU after treatment. This corresponded to only 0.04 ± 0.03 log reduction and 8.98% ± 5.97% reduction in bacterial count (Table 2). The pronounced inhibition observed in the presence of sodium azide clearly indicates that singlet oxygen is the primary reactive species responsible for bacterial inactivation.

These findings are consistent with the established photochemistry of chlorophyll-derived photosensitizers. Upon visible-light excitation, chlorophyllin undergoes intersystem crossing to a long-lived triplet state capable of transferring energy to molecular oxygen, resulting in singlet oxygen generation through a type II photodynamic pathway [25,28]. Similar singlet oxygen-dominated antibacterial mechanisms

Table 2. ROS scavenger assay demonstrating the role of singlet oxygen and hydroxyl radicals in the photodynamic antibacterial activity of chlorophyllin–$Ca_3(PO_4)_2$ nanohybrid against *S. typhimurium*. Results are expressed as mean CFU, log reduction, and percentage reduction.

Treatment	CFU (Mean ± STDEV)	Log reduction (Mean ± STDEV)	Reduction (%) (Mean ± STDEV)
Control	218.00 ± 12.96	0	0
Nanohybrid + Light + Mannitol	7.67 ± 1.21	1.46 ± 0.08	96.47 ± 0.60
Nanohybrid + Light + Sodium Azide	197.67 ± 2.16	0.04 ± 0.03	8.98 ± 5.97

have been reported for chlorophyllin-based and porphyrin-based photodynamic systems, where sodium azide significantly diminished antimicrobial activity while hydroxyl radical scavengers exerted only minor effects [20,26,27].

The mechanistic findings obtained from the ROS-scavenger assay are further supported by the complementary evidence presented in this study. AO/EtBr fluorescence staining revealed extensive membrane permeabilization following photodynamic treatment, while SEM analysis demonstrated severe morphological deformation and loss of cellular integrity. Furthermore, significant leakage of intracellular nucleic acids and proteins was observed, indicating disruption of the bacterial cell envelope. Together, these results demonstrate that ROS generated by photoactivated chlorophyllin induces oxidative damage to membrane lipids, proteins, and other essential cellular components, ultimately leading to irreversible bacterial cell death.

The short lifetime and limited diffusion distance of singlet oxygen suggest that PDI occurs primarily in the immediate vicinity of the photosensitizer. Although SEM images of the dried material revealed an aggregated nanohybrid morphology, effective antimicrobial activity was nevertheless achieved, indicating that bacterial cells were able to interact sufficiently with the nanohybrid surface under the experimental conditions employed. Consequently, ROS generated by immobilized chlorophyllin are likely to exert their effects locally at the particle–cell interface rather than through long-range diffusion. Importantly, this localized mode of action indicates that cellular uptake or internalization of the photosensitizer is not required for bacterial killing. Instead, oxidative damage occurs predominantly at the cell surface following exposure to ROS generated by the immobilized photosensitizer.

From a practical perspective, the absence of a requirement for photosensitizer uptake represents a significant advantage for food decontamination applications. The immobilized chlorophyllin remains associated with the calcium phosphate nanohybrid matrix while retaining potent antimicrobial activity, thereby reducing concerns associated with free photosensitizer exposure and potential chemical residues on treated produce. Combined with its demonstrated stability, negligible chlorophyllin release, and reusability over multiple treatment cycles, the nanohybrid platform offers a promising and consumer-compatible approach for photodynamic decontamination of FCP.

3.9. Live–Dead Staining of *S. typhimurium* Treated with Chlorophyllin–$Ca_3(PO_4)_2$ Nanohybrid

Bacterial viability following photodynamic treatment was assessed using AO/EtBr dual staining and fluorescence microscopy. Untreated control samples, which were not exposed to either the nanohybrid or visible light, predominantly exhibited green fluorescence, indicating intact bacterial membranes and high cellular viability, with only a few red-fluorescent cells observed (Fig. 7a,b). This confirmed minimal background cell death under control conditions.

On the contrary, samples irradiated in the presence of the chlorophyllin–$Ca_3(PO_4)_2$ nanohybrid displayed a pronounced shift from green to red fluorescence, accompanied by a substantial reduction in green fluorescence intensity (Fig. 7c,d). The dominant red fluorescence observed after treatment indicates extensive membrane damage and loss of bacterial viability following photodynamic activation. Similar green-to-red fluorescence transitions have been reported for a variety of photodynamic antimicrobial systems and are considered reliable indicators of irreversible membrane injury and bacterial cell death. Li et al. [38] demonstrated comparable fluorescence changes using AIEgen-based photosensitizers, while Garcez et al. [39] reported dominant red fluorescence in antibiotic-resistant *E. coli* following photodynamic treatment. Similar staining patterns have also been observed in biofilm-associated infections [40,41]. Collectively, these observations support red fluorescence as a robust indicator of severe bacterial injury and PDI.

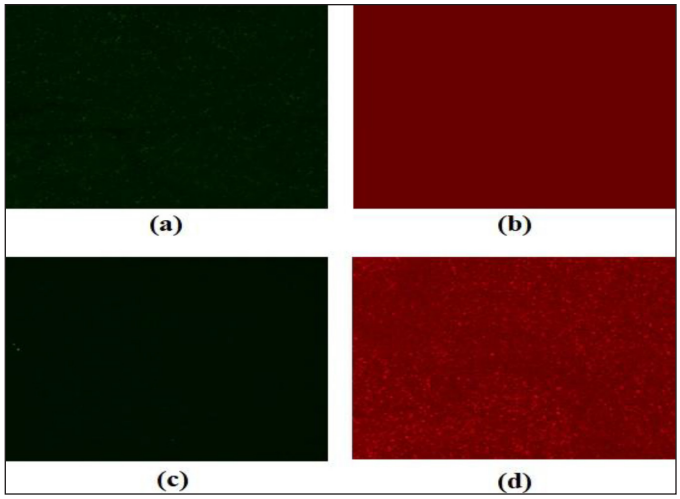

Figure 7. The live dead staining of *S. typhimurium:* (a) control without exposure to nanohybrid showing most of the bacterial cells live appearing in green color; (b) control without exposure to nanohybrid showing very few dead bacterial cells appearing in red color; (c) test after exposure to nanohybrid and light showing very few of the bacterial cells live appearing in green color; (d) test after exposure to nanohybrid and light showing most of the bacterial cells dead appearing in red color.

To provide semi-quantitative validation of the fluorescence microscopy observations, AO and EtBr fluorescence intensities were further measured using a multimode microplate reader. AO fluorescence served as an indicator of viable cells with intact membranes, whereas EtBr fluorescence reflected membrane-compromised or dead bacterial cells. Untreated control samples exhibited significantly higher corrected AO fluorescence intensity (6,391.65 ± 143.05) and minimal corrected EtBr fluorescence (49.58 ± 6.50), confirming the predominance of viable bacterial cells (Table 3). On the contrary, photodynamically treated samples showed a marked decrease in AO fluorescence (996.67 ± 20.93) together with a substantial increase in EtBr fluorescence (10,149.30 ± 460.75), indicating extensive membrane permeabilization following treatment ($p < 0.001$).

Table 3. Semi-quantitative AO/EtBr fluorescence analysis of photodynamically treated *S. typhimurium*.

Sample	Corrected AO fluorescence	Corrected EtBr fluorescence	Red/Green fluorescence ratio (EtBr/AO)	Live cells (%)	Dead cells (%)
Untreated control	6,391.65 ± 143.05	49.58 ± 6.50	0.008 ± 0.001	99.23 ± 0.12	0.77 ± 0.12
Chlorophyllin-$Ca_3(PO_4)_2$ nanohybrid + light	996.67 ± 20.93***	10,149.30 ± 460.75***	10.18 ± 0.34***	8.95 ± 0.28***	91.05 ± 0.28***

*Data are expressed as mean ± SD (n = 3). ***p < 0.001 compared with the untreated control.

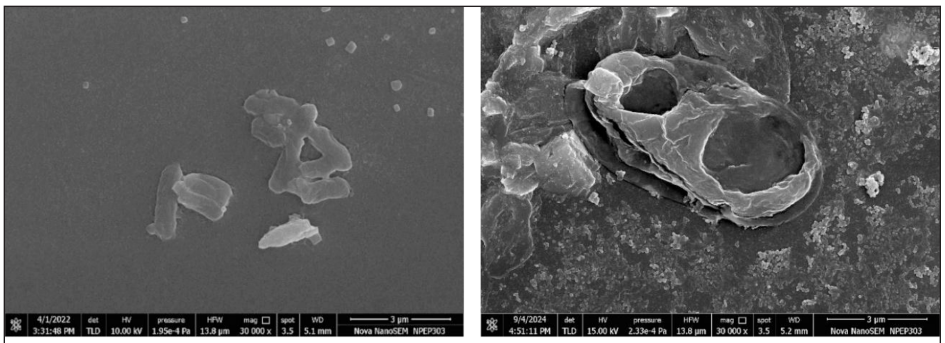

Figure 8. Scanning electron micrographs of *S. typhimurium*. (a) Untreated control cells showing intact rod-shaped morphology and smooth cell surfaces. (b) Cells treated with chlorophyllin–$Ca_3(PO_4)_2$ nanohybrid under visible-light irradiation show severe morphological damage, including surface deformation and loss of cellular integrity. Magnification: 30,000×; scale bar = 3 µm.

The red-to-green fluorescence ratio (EtBr/AO), which provides a quantitative measure of bacterial membrane integrity, increased dramatically from 0.008 ± 0.001 in untreated controls to 10.18 ± 0.34 in treated samples, representing an approximately 1,270-fold increase (p < 0.001). Fluorescence-derived viability analysis further revealed a significant decline in live bacterial populations from 99.23% ± 0.12% in untreated controls to 8.95% ± 0.28% following photodynamic treatment, whereas dead cell populations increased from 0.77% ± 0.12% to 91.05% ± 0.28% (p < 0.001) (Table 3).

The application of fluorescence analysis in the present study is consistent with recent advances in fluorescence-based bacterial viability assessment. He et al. [42] reported that ratiometric fluorescence sensing improves the accuracy and reliability of bacterial viability quantification by minimizing variability associated with absolute fluorescence measurements. Similarly, Wang et al. [43] demonstrated that fluorescence ratio-based approaches provide rapid and sensitive estimation of viable bacterial populations in complex environmental samples. In agreement with these reports, the substantial increase in the EtBr/AO fluorescence ratio observed in the present study quantitatively confirms the extensive bacterial damage induced by chlorophyllin-mediated photodynamic treatment. The pronounced increase in EtBr fluorescence further supports ROS-mediated membrane disruption as a major antibacterial mechanism. Upon visible-light activation, chlorophyllin generates singlet oxygen and other ROS that oxidatively damage membrane lipids, proteins, and nucleic acids, leading to loss of membrane integrity and enhanced EtBr uptake. Concurrently, the marked reduction in AO fluorescence reflects the depletion of viable bacterial cells following treatment. Collectively, the fluorescence microscopy observations and semi-quantitative fluorescence measurements strongly corroborate the CFU reduction, SEM analysis, intracellular leakage assay, and ROS scavenger studies, confirming that photoactivated chlorophyllin–$Ca_3(PO_4)_2$ nanohybrid induces extensive membrane disruption and irreversible bacterial cell death in *S. Typhimurium*.

3.10. Evaluation of Cell Membrane Integrity Following Photodynamic Treatment

Structural alterations in *S. typhimurium* following photodynamic treatment were examined using SEM. Untreated bacterial cells retained their characteristic rod-shaped morphology with smooth, intact surfaces (Fig. 8a). On the contrary, cells exposed to visible light in the presence of the chlorophyllin–$Ca_3(PO_4)_2$ nanohybrid exhibited pronounced morphological alterations, including surface collapse, membrane deformation, cellular shrinkage, and loss of structural integrity (Fig. 8b).

Although SEM images revealed pronounced surface deformation, membrane collapse, and loss of cellular integrity in treated cells, the observed morphological alterations alone cannot unequivocally distinguish ROS-induced membrane disruption from potential dehydration artifacts associated with SEM sample preparation. Therefore, SEM observations were interpreted in conjunction with the AO/EtBr fluorescence viability assay described in Section "Live-dead staining of *S. typhimurium* treated with chlorophyllin-$Ca_3(PO_4)_2$ nanohybrid". The substantial increase in EtBr fluorescence intensity and the approximately 1,270-fold increase in the EtBr/AO fluorescence ratio following photodynamic treatment demonstrated extensive membrane permeabilization, allowing selective penetration of EtBr into damaged bacterial cells. Furthermore, fluorescence-derived viability analysis indicated that more than 91% of the bacterial population was membrane-compromised following treatment. These findings provide independent evidence of membrane damage and support the interpretation that the morphological alterations observed by SEM are associated with genuine loss of membrane integrity rather than solely arising from sample preparation artifacts.

These ultrastructural disruptions are consistent with ROS-mediated oxidative stress generated upon chlorophyllin photoactivation via a type II photochemical pathway [7]. Singlet oxygen and other ROS are known to attack membrane lipids, proteins, and nucleic acids, ultimately leading to bacterial cell death [44]. Importantly, lethal

damage does not require internalization of the photosensitizer, as ROS generated at or near the cell surface are sufficient to induce membrane failure [8,45].

To further confirm membrane disruption, intracellular leakage assays were performed. Supernatants from untreated control samples exhibited negligible absorbance at 260 and 280 nm, indicating minimal release of nucleic acids or proteins. On the contrary, supernatants from photodynamically treated samples showed markedly increased absorbance (λ260 = 1.25; λ280 = 1.11), reflecting substantial leakage of intracellular components (Supporting Document Fig. 9).

The intracellular leakage results further complement the SEM and fluorescence-based membrane integrity analyses. Although SEM imaging does not permit definitive visualization of membrane pores at the magnifications employed, treated cells clearly exhibited membrane deformation, surface collapse, and loss of structural integrity. These morphological changes were accompanied by substantial leakage of intracellular constituents, as evidenced by the increased absorbance of the extracellular medium at 260 and 280 nm, corresponding to nucleic acids and proteins, respectively. Furthermore, AO/EtBr staining demonstrated extensive membrane permeabilization, with treated cells exhibiting markedly increased EtBr uptake and a significant increase in the EtBr/AO fluorescence ratio. Collectively, these independent observations indicate that photodynamic treatment compromises the bacterial membrane barrier, facilitating the release of intracellular biomolecules into the surrounding medium. The combined SEM, fluorescence, and leakage data therefore provide complementary evidence that membrane disruption is a major contributor to bacterial inactivation by the chlorophyllin–$Ca_3(PO_4)_2$ nanohybrid.

When considered together with the SEM observations and AO/EtBr membrane permeability analysis, the observed leakage of nucleic acids and proteins provides strong evidence that photodynamic treatment compromises membrane barrier function, resulting in loss of intracellular contents and ultimately bacterial cell death. Similar leakage patterns and membrane-disruption mechanisms have been reported for other chlorophyllin-based photodynamic antimicrobial systems [31].

3.11. Decontamination of FCP

Treatment of cucumber slices with free chlorophyllin solution resulted in incomplete microbial inactivation and noticeable surface staining (Supporting document Fig. 10), highlighting a common limitation for consumer acceptability [46,47]. On the contrary, cucumbers treated with the chlorophyllin–$Ca_3(PO_4)_2$ nanohybrid showed no visible staining, indicating reduced photosensitizer migration and improved aesthetic compatibility. The enhanced performance of the nanohybrid is attributed to chlorophyllin immobilization within the calcium phosphate matrix, which improves photostability, localizes ROS generation at the microbial interface, and minimizes diffusion into plant tissues. Similar advantages have been reported for chlorophyllin incorporated in Ca–P matrices in non-food systems [48]. Unlike light-only treatments requiring prolonged exposure for partial inactivation [49], the nanohybrid achieved complete bacterial inactivation under mild illumination. Furthermore, the insoluble nanohybrid can be recovered and reused, unlike free chlorophyllin, aligning with industry demands for cost-effective and sustainable photodynamic decontamination [9,50].

To further assess the practical applicability of the developed photodynamic system, additional experiments were conducted against naturally occurring microbial populations associated with fresh produce surfaces. Unlike inoculated pathogen studies, these experiments better represent real-world fresh-produce contamination,

Table 4. Photodynamic decontamination of fresh-produce-associated natural microflora using chlorophyllin–$Ca_3(PO_4)_2$ nanohybrid under visible-light irradiation.

Produce	Log reduction (Mean ± STDEV)	Reduction (%) (Mean ± STDEV)
Cucumber	1.75 ± 0.14	98.14 ± 0.56
Cabbage	2.03 ± 0.29	99.08 ± 0.94
Spinach	1.94 ± 0.12	98.82 ± 0.32

where heterogeneous microbial communities comprising spoilage organisms and environmental microorganisms coexist on produce surfaces. For cucumber-associated natural microflora, the untreated samples exhibited an average microbial count of 160.67 ± 6.66 CFU, whereas photodynamic treatment with chlorophyllin–$Ca_3(PO_4)_2$ nanohybrid reduced the count to 3.00 ± 1.0 CFU. This corresponded to a mean log reduction of 1.75 ± 0.14 log CFU and a percentage reduction of 98.14% ± 0.56% (Table 4). The reduction was statistically significant compared with the untreated control ($p < 0.001$). These findings indicate that the antimicrobial activity of the nanohybrid is not restricted to *S. typhimurium* but extends to mixed microbial populations naturally present on cucumber surfaces.

To evaluate whether the effectiveness of the nanohybrid was influenced by the surface characteristics of the produce, naturally occurring microflora recovered from cabbage and spinach leaves were also examined. Leafy vegetables generally possess more complex surface architectures, including folds, veins, stomata, and microscopic crevices that can facilitate microbial attachment and reduce the efficacy of conventional decontamination treatments. Nevertheless, photodynamic treatment reduced cabbage-associated microbial counts from 213.00 ± 12.53 CFU to 2.00 ± 2.0 CFU, corresponding to a 2.03 ± 0.29 log reduction and 99.08% ± 0.94% reduction in viable microorganisms. Similarly, spinach-associated microflora decreased from 590.33 ± 19.66 CFU to 7.00 ± 2.0 CFU following treatment, corresponding to a 1.94 ± 0.12 log reduction and 98.82% ± 0.32% reduction (Table 4). In both cases, the reductions were highly significant compared with the untreated controls ($p < 0.001$).

The consistent antimicrobial performance observed across cucumber, cabbage, and spinach demonstrates that the photodynamic efficacy of chlorophyllin–$Ca_3(PO_4)_2$ nanohybrid is largely maintained despite substantial differences in produce surface morphology and naturally occurring microbial communities. The antimicrobial activity is attributed to visible-light activation of immobilized chlorophyllin, which generates ROS capable of inducing oxidative damage to microbial membranes, proteins, and nucleic acids. Furthermore, immobilization within the calcium phosphate nanohybrid matrix likely enhances photosensitizer stability, minimizes leaching, and promotes sustained photodynamic activity, thereby improving microbial inactivation efficiency. Collectively, these findings demonstrate that chlorophyllin–$Ca_3(PO_4)_2$ nanohybrid is effective not only against inoculated *S. typhimurium* but also against naturally occurring microbial populations present on a variety of fresh-produce surfaces.

A potential limitation of the present study is that the inoculated pathogen decontamination experiments were conducted using surface-associated bacterial populations and did not specifically evaluate microorganisms residing within stomata, epidermal crevices, or internalized plant tissues. Such protected microenvironments are known to reduce the effectiveness of many produce sanitization strategies because antimicrobial agents may have limited access to deeply embedded cells. Furthermore, in the assessment of natural produce-associated microflora, microorganisms were first detached

from cucumber, cabbage, and spinach surfaces into PBS prior to photodynamic treatment. Consequently, the observed microbial reductions demonstrate the antimicrobial efficacy of the chlorophyllin–$Ca_3(PO_4)_2$ nanohybrid against produce-associated microorganisms but do not directly establish its ability to inactivate bacteria located within stomatal cavities or other protected plant microstructures. Because ROS generated during photodynamic treatment are short-lived and act primarily near the site of generation, bacterial accessibility to the photosensitizer remains an important factor influencing treatment efficacy. Future studies employing fluorescently labeled bacteria, confocal laser scanning microscopy, or artificial internalization models would be valuable for determining the effectiveness of the nanohybrid system against microorganisms residing within stomata and other protected plant microenvironments. Despite this limitation, the observed antimicrobial efficacy against both inoculated pathogens and naturally occurring produce-associated microflora highlights the potential of chlorophyllin–$Ca_3(PO_4)_2$ nanohybrid as a sustainable photodynamic decontamination strategy for fresh-cut fruits and vegetables.

Although the optimized photodynamic treatment required 25 minutes of visible-light exposure to achieve maximum antimicrobial efficacy under the laboratory conditions employed in this study, further reduction of treatment time may be feasible for industrial implementation. In photodynamic systems, microbial inactivation is primarily governed by the total light dose delivered to the photosensitizer. Consequently, increasing light intensity, improving light distribution, reducing the distance between the light source and the produce surface, or employing high-power LED arrays may significantly shorten the required exposure time while maintaining equivalent antimicrobial performance. In addition, commercial fresh-produce processing operations commonly utilize thin product layers, conveyor-based transport systems, and continuous illumination chambers, which can enhance light penetration and photosensitizer activation. The relatively rapid ROS generation observed in the present study suggests that process optimization through engineering modifications could further improve treatment throughput. Future studies should therefore focus on evaluating higher illumination intensities, continuous-flow treatment configurations, and pilot-scale processing systems to establish the industrial feasibility of chlorophyllin–$Ca_3(PO_4)_2$ nanohybrid-mediated photodynamic decontamination.

Although the present study primarily focused on microbial decontamination efficacy, no visible discoloration, staining, or surface damage was observed on cucumber, cabbage, or spinach samples following photodynamic treatment. Since preservation of product quality is a critical consideration for fresh-produce applications, future studies should include instrumental evaluation of texture, firmness, color, chlorophyll retention, and storage stability to comprehensively assess the impact of chlorophyllin–$Ca_3(PO_4)_2$ nanohybrid on produce quality during post-treatment storage.

3.12. Stability and Retention of Chlorophyllin Within the $Ca_3(PO_4)_2$ Nanohybrid

The absorbance values measured in the supernatants remained very low throughout the incubation period, indicating negligible chlorophyllin release from the chlorophyllin–$Ca_3(PO_4)_2$ nanohybrid. A small increase in absorbance was observed during the initial stages of incubation, which may correspond to the release of weakly surface-associated chlorophyllin. Subsequently, a slight decrease in absorbance was observed at later time points (Table 5). Because the absorbance values were close to the detection limit, these fluctuations are likely influenced by analytical variation and/or gradual degradation of trace amounts of released chlorophyllin in aqueous solution. Overall, the results demonstrate strong retention of chlorophyllin within the calcium phosphate matrix and support the stability of the nanohybrid under the tested conditions.

Table 5. Absorbance of PBS supernatants collected after repeated washing cycles of chlorophyllin–$Ca_3(PO_4)_2$ nanohybrid. Measurements at 405 nm were used as a qualitative indicator of chlorophyllin presence in the supernatant and to assess immobilization stability.

Incubation time (h)	Absorbance at 405 (nm)
24	0.007
48	0.035
72	0.017
96	0.006
120	0.001

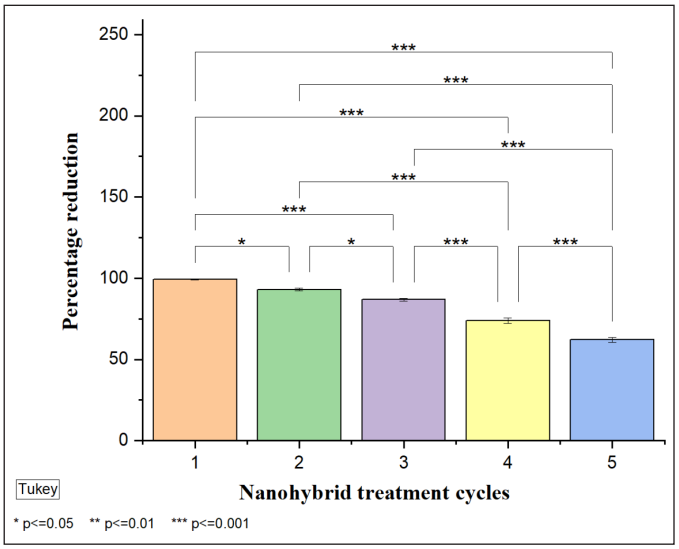

Figure 9. Reusability of chlorophyllin–$Ca_3(PO_4)_2$ nanohybrid for PDI of *S. typhimurium* over five consecutive cycles. Antibacterial activity is expressed as a percentage reduction in viable bacterial counts relative to the untreated control. Error bars represent SD (n = 3).

3.13. Reusability of Chlorophyllin–$Ca_3(PO_4)_2$ Nanohybrid for Photodynamic Antibacterial Inactivation

The practical applicability of photosensitizer-based antimicrobial systems depends not only on their antibacterial efficacy but also on their operational stability and potential for repeated use. Therefore, the reusability of chlorophyllin–$Ca_3(PO_4)_2$ nanohybrid was evaluated through five consecutive PDI cycles against *S. typhimurium*.

The recovered chlorophyllin–$Ca_3(PO_4)_2$ nanohybrid retained substantial photodynamic antibacterial activity during repeated reuse cycles against *S. typhimurium*. The first cycle exhibited the highest efficacy, resulting in a 99.27% ± 0.66% reduction in viable bacterial counts. A gradual decline in antimicrobial performance was observed with successive reuse cycles; however, significant bacterial inactivation was maintained throughout the study. Percentage reductions of 93.06% ± 1.35%, 86.78% ± 1.55%, 73.91% ± 2.82%, and 62.11% ± 2.70% were achieved during the second, third, fourth, and fifth cycles, respectively (Fig. 9). The progressive reduction in antibacterial efficacy over successive cycles may be attributed to partial loss of active surface sites, gradual photobleaching of immobilized chlorophyllin molecules, or minor

material losses during recovery and washing steps. Nevertheless, the nanohybrid remained capable of achieving appreciable bacterial inactivation even after five consecutive cycles, demonstrating the strong association of chlorophyllin with the calcium phosphate matrix and supporting the stability and recyclability of the developed photodynamic system. These findings provide direct evidence that the immobilized photosensitizer retains functional activity upon reuse, thereby addressing a key limitation of free chlorophyllin, which cannot be readily recovered and reused following treatment.

It is noteworthy that the initial antibacterial activity of free chlorophyllin and chlorophyllin–$Ca_3(PO_4)_2$ nanohybrid was found to be comparable under the optimized photodynamic treatment conditions described in this study. Therefore, the primary advantage of nanohybrid formation is not necessarily an increase in immediate antibacterial efficacy but rather the immobilization of the photosensitizer within a recoverable inorganic matrix. Free chlorophyllin remains dissolved in the treatment medium after photodynamic treatment and cannot be readily separated for reuse. Consequently, fresh photosensitizers must be supplied for each treatment cycle, which may increase material consumption and operational costs.

On the contrary, immobilization within the calcium phosphate nanohybrid matrix enables facile recovery of chlorophyllin by simple centrifugation and allows repeated photodynamic application while retaining substantial antibacterial activity. The ability to recover and reuse the photosensitizer represents a significant practical advantage, particularly for food decontamination applications where large treatment volumes may be required. Furthermore, the sustained antibacterial performance observed over multiple cycles is consistent with the low chlorophyllin leaching values reported in Section "Stability and retention of chlorophyllin within the $Ca_3(PO_4)_2$ nanohybrid", indicating that a substantial fraction of the immobilized chlorophyllin remained associated with the nanohybrid structure during repeated use.

From an application perspective, reusability is a key factor influencing process economics and sustainability. The ability to repeatedly utilize the same photosensitizer-containing material reduces chlorophyllin consumption, minimizes waste generation, and lowers the likelihood of residual photosensitizer accumulation in treated systems. Collectively, these findings demonstrate that chlorophyllin–$Ca_3(PO_4)_2$ nanohybrid retains significant photodynamic antibacterial activity after repeated use and provides a practical advantage over free chlorophyllin through enhanced recoverability and operational reusability.

Although the present study demonstrated effective antimicrobial activity and low chlorophyllin leaching, the amount of residual nanohybrid remaining on produce surfaces after treatment was not quantitatively determined. Nevertheless, the total quantity of nanohybrid applied during treatment was low (10 mg), and both constituent materials, calcium phosphate and chlorophyllin, possess favorable food-compatibility profiles. Calcium phosphate is widely used in food and nutraceutical applications, while chlorophyllin is a food-grade chlorophyll derivative. Future studies should investigate nanohybrid wash-off behavior and residual surface deposition following treatment and rinsing to further assess consumer exposure under practical processing conditions.

4. CONCLUSION

This study demonstrates that calcium phosphate can serve as an effective immobilization matrix for chlorophyllin, producing a stable food-compatible photodynamic nanohybrid with high EE and minimal chlorophyllin release. Structural characterization revealed that antimicrobial performance was achieved despite the absence of highly ordered flower-like architectures, indicating that efficient chlorophyllin–calcium phosphate integration is more critical than morphological complexity for photodynamic function.

Upon visible-light activation, the chlorophyllin–$Ca_3(PO_4)_2$ nanohybrid exhibited strong antibacterial activity against both gram-negative and gram-positive bacteria, including *S. typhimurium*, *S. aureus*, and *B. subtilis*. Mechanistic investigations combining ROS scavenger assays, fluorescence-based viability analysis, SEM observations, and intracellular leakage studies demonstrated that bacterial inactivation occurs primarily through singlet oxygen-mediated oxidative damage to the cell envelope, resulting in loss of membrane integrity and irreversible cell death. The findings further indicate that direct uptake of the photosensitizer by bacterial cells is not required for antimicrobial activity, as localized ROS generation at the particle–cell interface is sufficient to induce lethal damage.

The nanohybrid also effectively reduced naturally occurring microflora recovered from cucumber, cabbage, and spinach surfaces. Unlike free chlorophyllin, the immobilized photosensitizer could be recovered and reused while retaining substantial antibacterial activity over multiple treatment cycles, highlighting the practical advantages of the nanohybrid approach for repeated applications.

Overall, the developed chlorophyllin–$Ca_3(PO_4)_2$ nanohybrid represents a promising photodynamic decontamination platform that combines antimicrobial efficacy, operational stability, reusability, and food-safety compatibility. Future work should focus on direct surface decontamination studies on intact produce, optimization of illumination conditions for industrial implementation, and evaluation of product quality attributes, including texture, color, nutritional quality, and shelf-life following treatment.

5. LIST OF ABBREVIATIONS

CFU, colony-forming units; FCP, fresh-cut produce; PBS, phosphate-buffered saline; ROS, reactive oxygen species; SEM, scanning electron microscopy; XRD, X-ray diffraction.

6. ACKNOWLEDGMENT

Ms. Manisha Shinde acknowledges the Indian Council of Medical Research for providing her fellowship and the Department of Microbiology, Savitribai Phule Pune University (SPPU; formerly the University of Pune), Pune, for providing the necessary research facilities. Dr. Umesh Jadhav gratefully acknowledges the Indian Council of Medical Research for funding this research under Project ID 2021-10581 (Reference No. 35/13/2022-NANO/BMS, dated 18 January 2023). The authors also acknowledge the Central Instrumentation Facility, Savitribai Phule Pune University, for providing instrumental support.

7. AUTHOR CONTRIBUTIONS

All authors made substantial contributions to conception and design, acquisition of data, or analysis and interpretation of data; took part in drafting the article or revising it critically for important intellectual content; agreed to submit to the current journal; gave final approval of the version to be published; and agreed to be accountable for all aspects of the work. All the authors are eligible to be authors as per the International Committee of Medical Journal Editors (ICMJE) requirements/guidelines.

8. CONFLICTS OF INTEREST

The authors report no financial or any other conflicts of interest in this work.

9. ETHICAL APPROVALS

This study does not involve experiments on animals or human subjects.

10. DATA AVAILABILITY

All the data are available with the authors and shall be provided upon request.

11. PUBLISHER'S NOTE

All claims expressed in this article are solely those of the authors and do not necessarily represent those of the publisher, the editors, or the reviewers. This journal remains neutral with regard to jurisdictional claims in published institutional affiliation.

12. DECLARATION OF AI-ASSISTED TECHNOLOGIES

During the preparation of the revised manuscript, the authors used an AI-assisted language tool solely to improve grammar, language quality, readability, and scientific presentation. No AI tool was used to generate experimental data, perform analyses, interpret results, draw conclusions, or create scientific content. The authors reviewed and edited the content and take full responsibility for the published work.

13. SUPPLEMENTARY MATERIAL

The supplementary material can be accessed at the journal's website: https://jabonline.in/admin/php/uploadss/1509_pdf.pdf

REFERENCES

1. Bhilwadikar T, Pounraj S, Manivannan S, Rastogi NK, Negi PS. Decontamination of microorganisms and pesticides from fresh fruits and vegetables: a comprehensive review from common household processes to modern techniques. Compr Rev Food Sci Food Saf 2019;18(04):1003–38; doi: https://doi.org/10.1111/1541-4337.12453
2. Yousuf O, Titikshya S, Singh A. Fresh-cut fruits and vegetables: scope in developing countries and approaches to improve quality and safety. Int J Chem Stud 2018;6(03):2226–9.
3. Callejón RM, Rodríguez-Naranjo MI, Ubeda C, Hornedo-Ortega R, Garcia-Parrilla MC, Troncoso AM. Reported foodborne outbreaks due to fresh produce in the United States and European Union: trends and causes. Foodborne Pathog Dis 2015;12(01):32–8; doi: https://doi.org/10.1089/fpd.2014.1821
4. World Health Organization. WHO estimates of the global burden of foodborne diseases: foodborne disease burden epidemiology reference group 2007–2015 [Internet]. World Health Organization, Geneva, Switzerland, 2015. Available via https://www.who.int/publications/i/item/9789241565165 (Accessed 30 January 2026)
5. Deng LZ, Mujumdar AS, Pan Z, Vidyarthi SK, Xu J, Zielinska M, *et al.* Emerging chemical and physical disinfection technologies of fruits and vegetables: a comprehensive review. Crit Rev Food Sci Nutr 2020;60(15):2481–508; doi: https://doi.org/10.1080/10408398.2019.1649633
6. Ölmez H, Kretzschmar U. Potential alternative disinfection methods for organic fresh-cut industry for minimizing water consumption and environmental impact. LWT Food Sci Technol 2009;42(03):686–93; doi: https://doi.org/10.1016/j.lwt.2008.08.001
7. Wainwright M, Maisch T, Nonell S, Plaetzer K, Almeida A, Tegos GP, *et al.* Photoantimicrobials—are we afraid of the light?. Lancet Infect Dis 2017;17(02):e49–55; doi: https://doi.org/10.1016/S1473-3099(16)30268-7
8. Sperandio FF, Huang YY, Hamblin MR. Antimicrobial photodynamic therapy to kill gram-negative bacteria. Recent Pat Antiinfect Drug Discov 2013;8(2):108–20; doi: https://doi.org/10.2174/1574891x113089990012
9. Luksiene Z, Paskeviciute E. Novel approach to the microbial decontamination of strawberries: chlorophyllin-based photosensitization. J Appl Microbiol 2011;110(05):1274–83; doi: https://doi.org/10.1111/j.1365-2672.2011.04986.x
10. Zhang Y, Ding Z, Shao C, Xie J. Chlorophyllin-based 405 nm light photodynamic improved fresh-cut pakchoi quality at postharvest and inhibited the formation of biofilm. Foods. 2022;11(16):2541. doi:10.3390/foods11162541.
11. Wang X, Shi J, Li Z, Zhang S, Wu H, Jiang Z, *et al.* Facile one-pot preparation of chitosan/calcium pyrophosphate hybrid microflowers. ACS Appl Mater Inter 2014;6(16):14522–32; doi: https://doi.org/10.1021/am503787h
12. Shende P, Kasture P, Gaud RS. Nanoflowers: the future trend of nanotechnology for multi-applications. Artif Cells Nanomed Biotechnol 2018;46(sup1):413–22; doi: https://doi.org/10.1080/21691401.2018.1428812
13. Yin Y, Xiao Y, Lin G, Xiao Q, Lin Z, Cai Z. An enzyme–inorganic hybrid nanoflower based immobilized enzyme reactor with enhanced enzymatic activity. J Mater Chem B. 2015;3:2295–2300. doi:10.1039/C4TB01697A
14. Demirbas A, Welt BA, Ocsoy I. Biosynthesis of red cabbage extract directed Ag NPs and their effect on the loss of antioxidant activity. Mater Lett 2016;179:20–3; doi: https://doi.org/10.1016/j.matlet.2016.05.056
15. Kilic A, Altınkaynak C, Ildiz N, Ozdemir N, Yilmaz V, Ocsoy I. A new approach for green synthesis and characterization of *Artemisia* L. (Asteraceae) genotype extracts–Cu^{2+} nanocomplexes (nanoflower) and their effective antimicrobial activity. Med-Science 2020;9(01):191–196; doi: https://doi.org/10.5455/medscience.2019.08.9165
16. Cao P, Wu X, Zhang W, Zhao L, Sun W, Tang Z. Killing oral bacteria using metal–organic frameworks. Ind Eng Chem Res 2020;59(04):1559–67; doi: https://doi.org/10.1021/acs.iecr.9b05659
17. Luan L, Du L, Shi W, Li Y, Zhang Q. Photodynamic inactivation of bacteria and biofilms with benzoselenadiazole-doped metal-organic frameworks. Molecules 2022;27(24):8908; doi: https://doi.org/10.3390/molecules27248908
18. Du L, Shi W, Hao X, Luan L, Wang S, Lu J, *et al.* Synergistic photodynamic/antibiotic therapy with photosensitive MOF-based nanoparticles to eradicate bacterial biofilms. Pharmaceutics 2023;15(07):1826; doi: https://doi.org/10.3390/pharmaceutics15071826
19. Mei L, Zhang Y, Wang K, Chen S, Song T. Nanomaterials at the forefront of antimicrobial therapy by photodynamic and photothermal strategies. Mater Today Bio 2024;29:101354; doi: https://doi.org/10.1016/j.mtbio.2024.101354
20. Yu Q, Wang C, Zhang X, Chen H, Wu MX, Lu M. Photochemical strategies toward precision targeting against multidrug-resistant bacterial infections. ACS Nano 2024;18(22):14085–122; doi: https://doi.org/10.1021/acsnano.3c12714
21. Yu Z, Fu X, Lucas T, Zhao H, Chen C, Dubail I, *et al.* MOF-enhanced phototherapeutic wound dressings against drug-resistant bacteria. Adv Healthcare Mater 2025;14:1–4; doi: https://doi.org/10.1002/adhm.202402418
22. Yan X, Lin Z, Shen H, Chen Y, Chen L. Photo-responsive antibacterial metal organic frameworks. J Mater Chem B 2025;13:6299–316; doi: https://doi.org/10.1039/D5TB00105F
23. Epple M, Ganesan K, Heumann R, Klesing J, Kovtun A, Neumann S, *et al.* Application of calcium phosphate nanoparticles in biomedicine. J Mater Chem 2010;20(01):18–23; doi: https://doi.org/10.1039/B910885h
24. Nakamura M, Bunryo W, Narazaki A, Oyane A. High immobilization efficiency of basic protein within heparin-immobilized calcium phosphate nanoparticles. Int J Mol Sci 2022;23(19):11530; doi: https://doi.org/10.3390/ijms231911530

25. Hamblin MR, Hasan T. Photodynamic therapy: a new antimicrobial approach to infectious disease?. Photochem Photobiol Sci 2004;3(05):436–50; doi: https://doi.org/10.1039/B311900A
26. Maisch T. Anti-microbial photodynamic therapy: useful in the future?. Lasers Med Sci 2007;22(02):83–91; doi: https://doi.org/10.1007/s10103-006-0409-7
27. Liu D, Gu W, Wang L, Sun J. Photodynamic inactivation and its application in food preservation. Crit Rev Food Sci Nutr 2023;63(14):2042–56; doi: https://doi.org/10.1080/10408398.2021.1969892
28. Foote CS. Definition of type I and type II photosensitized oxidation. Photochem Photobiol 1991;54(05):659; doi: https://doi.org/10.1111/j.1751-1097.1991.tb02071.x
29. Tawre MS, Kamble EE, Kumkar SN, Mulani MS, Pardesi KR. Antibiofilm and antipersister activity of acetic acid against extensively drug resistant *Pseudomonas aeruginosa* PAW1. PLoS One 2021;16(02):246020; doi: https://doi.org/10.1371/journal.pone.0246020
30. Trevisan DAC, Silva AFD, Negri M, Abreu Filho BAD, Machinski Junior M, Patussi EV, *et al.* Antibacterial and antibiofilm activity of carvacrol against *Salmonella enterica* serotype typhimurium. Braz J Pharm Sci 2018;54(01):e17229; doi: https://doi.org/10.1590/s2175-97902018000117229
31. Buchovec I, Lukseviciute V, Marsalka A, Reklaitis I, Luksiene Z. Effective photosensitization-based inactivation of gram (−) food pathogens and molds using the chlorophyllin–chitosan complex. Photochem Photobiol Sci 2016;15(04):506–16; doi: https://doi.org/10.1039/c5pp00376h
32. Ge J, Lei J, Zare RN. Protein–inorganic hybrid nanoflowers. Nat Nanotechnol 2012;7(07):428–32; doi: https://doi.org/10.1038/nnano.2012.80
33. Somturk B, Yilmaz I, Altinkaynak C, Karatepe A, Özdemir N, Ocsoy I. Synthesis of urease hybrid nanoflowers and their enhanced catalytic properties. Enzyme Microb Technol 2016;86:134–42; doi: https://doi.org/10.1016/j.enzmictec.2015.09.005
34. Nadar SS, Gawas SD, Rathod VK. Self-assembled organic–inorganic hybrid glucoamylase nanoflowers with enhanced activity and stability. Int J Biol Macromol 2016;92:660–9; doi: https://doi.org/10.1016/j.ijbiomac.2016.06.071
35. Altinkaynak C, Tavlasoglu S, Ÿzdemir N, Ocsoy I. A new generation approach in enzyme immobilization: organic–inorganic hybrid nanoflowers with enhanced catalytic activity and stability. Enzyme Microb Technol 2016;93–94:105–12; doi: https://doi.org/10.1016/j.enzmictec.2016.06.011
36. Nitzan Y, Pechatnikov I. Approaches to kill gram-negative bacteria by photosensitized processes. In: Hamblin MR, Jori G (eds.). Photodynamic inactivation of microbial pathogens: medical and environmental applications, Royal Society of Chemistry, Cambridge, UK, p 45, 2011; doi: https://doi.org/10.1039/BK9781849731447-00045
37. Aponiene K, Luksiene Z. Effective combination of LED-based visible light, photosensitizer and photocatalyst to combat gram (−) bacteria. J Photochem Photobiol B 2015;142:257–63; doi: https://doi.org/10.1016/j.jphotobiol.2014.11.011
38. Li Y, Pan T, Peng K, Huang Y, Li W, Liu FS, *et al.* Synergistic antibacterial strategy of AIEgens photosensitizer CPTQ for photodynamic therapy and ferroptosis-like bacterial death to prevent dental caries. ACS Appl Mater Inter 2025;17(35):49165–82; doi: https://doi.org/10.1021/acsami.5c08578
39. Garcez AS, Kaplan M, Jensen GJ, Scheidt FR, Oliveira EM, Suzuki SS. Effects of antimicrobial photodynamic therapy on antibiotic-resistant *Escherichia coli*. Photodiagnosis Photodyn Ther 2020;32:102029; doi: https://doi.org/10.1016/j.pdpdt.2020.102029
40. Santana AP, Cunha DM, Piazza RD, Wainwright M, Feres M, Retamal-Valdes B, *et al.* Butyl toluidine blue as a photosensitizer for antimicrobial photodynamic therapy on titanium-associated biofilms. J Photochem Photobiol B 2025;273:113274; doi: https://doi.org/10.1016/j.jphotobiol.2025.113274
41. Ye Y, He J, Qiao Y, Qi Y, Zhang H, Santos HA, *et al.* Mild temperature photothermal assisted anti-bacterial and anti-inflammatory nanosystem for synergistic treatment of post-cataract surgery endophthalmitis. Theranostics 2020;10(19):8541–57; doi: https://doi.org/10.7150/thno.46895
42. He S, Chen Y, Wang J, Sun J, Zhang X, Chen Q. Rapid and sensitive quantification of bacterial viability using ratiometric fluorescence sensing. Anal Chem 2024;96:11018–25; doi: https://doi.org/10.1021/acs.analchem.4c01737
43. Wang M, Ateia M, Hatano Y, Miyanaga K, Yoshimura C. Novel fluorescence-based method for rapid quantification of live bacteria in river water and treated wastewater. Environ Sci Adv 2022;1:30–6; doi: https://doi.org/10.1039/d1va00017a
44. Cieplik F, Deng D, Crielaard W, Buchalla W, Hellwig E, Al-Ahmad A, *et al.* Antimicrobial photodynamic therapy – what we know and what we don't. Crit Rev Microbiol 2018;44(05):571–89; doi: https://doi.org/10.1080/1040841X.2018.1467876
45. Krüger M, Richter P, Strauch SM, Nasir A, Burkovski A, Antunes CA, *et al.* What an *Escherichia coli* mutant can teach us about the antibacterial effect of chlorophyllin. Microorganisms 2019;7(02):59; doi: https://doi.org/10.3390/microorganisms7020059
46. Luksiene Z, Buchovec I. Impact of chlorophyllin–chitosan coating and visible light on the microbial contamination, shelf life, nutritional and visual quality of strawberries. Innov Food Sci Emerg Technol 2019;52:463–72; doi: https://doi.org/10.1016/j.ifset.2019.02.003
47. López-Carballo G, Hernández-Muñoz P, Gavara R, Ocio MJ. Photoactivated chlorophyllin-based gelatin films and coatings to prevent microbial contamination of food products. Int J Food Microbiol 2008;126(1–2):65–70; doi: https://doi.org/10.1016/j.ijfoodmicro.2008.05.002
48. Zhang ZY, An YL, Wang XS, Cui LY, Li SQ, Liu CB, *et al. In vitro* degradation, photo-dynamic and thermal antibacterial activities of Cu-bearing chlorophyllin-induced Ca–P coating on magnesium alloy AZ31. Bioact Mater 2022;18:284–99; doi: https://doi.org/10.1016/j.bioactmat.2022.01.050
49. Josewin SW, Kim MJ, Yuk HG. Inactivation of Listeria monocytogenes and *Salmonella* spp. on cantaloupe rinds by blue light emitting diodes (LEDs). Food Microbiol 2018;76:219–25; doi: https://doi.org/10.1016/j.fm.2018.05.012
50. Paskeviciute E, Zudyte B, Luksiene Z. Towards better microbial safety of fresh produce: chlorophyllin-based photosensitization for microbial control of foodborne pathogens on cherry tomatoes. J Photochem Photobiol B 2018;182:130–6; doi: https://doi.org/10.1016/j.jphotobiol.2018.04.009

How to cite this article:
Shukla S, Shinde M, Lade A, Jagtap S, Pai S, Gupta G, Satpute S, Jadhav U. Visible-light-activated chlorophyllin–calcium phosphate nanohybrid for reusable photodynamic decontamination of fresh-cut produce. J Appl Biol Biotech 2026;14(6):49-64. DOI: 10.7324/jabb.2026.310917